Research Square

Preprints are preliminary reports that have not undergone peer review.
They should not be considered conclusive, used to inform clinical practice,
or referenced by the media as validated information.

Low Complexity Sparse Beamspace DOA Estimation Via Single Measurement Vectors for Uniform Circular Array

Di Zhao (zhaodi820@bupt.edu.cn)
Beijing University of Posts and Telecommunications https://orcid.org/0000-0003-4527-338X
Weijie Tan
Guizhou University
Zhongliang Deng
Beijing University of Posts and Telecommunications
Gang Li
CETC 54th Research Institute: China Electronics Technology Group Corp 54th Research Institute

Research

Keywords: Direction-of-arrival estimation, uniform circular array, low complexity, beamspace transformation, convex optimization

Posted Date: March 15th, 2021

DOI: https://doi.org/10.21203/rs.3.rs-278792/v1

License: This work is licensed under a Creative Commons Attribution 4.0 International License.
Read Full License

Version of Record: A version of this preprint was published at EURASIP Journal on Advances in Signal Processing on July 30th, 2021. See the published version at https://doi.org/10.1186/s13634-021-00770-2.

RESEARCH

Low Complexity Sparse Beamspace DOA Estimation via Single Measurement Vectors for Uniform Circular Array

Di Zhao[1,2*], Weijie Tan[3], Zhongliang Deng[1] and Gang Li[2]

*Correspondence:
zhaodi820@bupt.edu.cn
[1]Wireless Network Positioning and Communication Integration Research Center, School of Electronic Engineering, Beijing University of Posts and Telecommunications, Beijing, 100876 China
Full list of author information is available at the end of the article

Abstract

In this paper, we present a low complexity beamspace direction-of-arrival (DOA) estimation method for uniform circular array (UCA), which is based on the single measurement vectors (SMVs) via vectorization of sparse covariance matrix. In the proposed method, we firstly transform the signal model of UCA to that of virtual uniform linear array (ULA) in beamspace domain using the beamspace transformation (BT). Subsequently, by applying the vectorization operator on the virtual ULA-like array signal model, a new dimension-reduction array signal model consists of SMVs based on Khatri-Rao (KR) product is derived. And then, the DOA estimation is converted to the convex optimization problem. Finally, simulations are carried out to verify the effectiveness of the proposed method, the results show that without knowledge of the signal number, the proposed method not only has higher DOA resolution than subspace-based methods in low signal-to-noise ratio (SNR), but also has much lower computational complexity comparing other sparse-like DOA estimation methods.

Keywords: Direction-of-arrival estimation; uniform circular array; low complexity; beamspace transformation; convex optimization

1 Introduction

In the past decades, direction-of-arrival (DOA) estimation of propagating plane waves for uniform circular array (UCA) has been widely used in various fields, such as communication, radar, sonar, radio astronomy and so on [1]. The DOA estimation algorithms and their derivatives are divided into three categories: Beamforming techniques [2, 3], subspace-based methods [4, 5], the maximum likelihood approach [6,7]. Besides these approaches, sparse-representation-based DOA estimation approaches [8–11] have been paid great attention in recent years, which are widely used in element-space domain, beamspace domain [12] and various scenarios where mixture (coherent and incoherent, or circular and noncircular [13, 14]) signals exist as well. The sparse-representation-based DOA estimation approaches are different from the conventional representative methods, such as the Capon beamformer [15] and the multiple signal classification (MUSIC) [16, 17]. In conventional DOA methods, the observation data model are generally treated as a linear combination of the steering vectors and incoming signals plus stochastic noise [18]. The sparse-based DOA estimation approaches are based on a sparse representation of observation data with an overcomplete basis, which comprised of spatial samples from the array manifold [10] on the premise that the DOAs of signals fall sparsely

into the entire spatial domain. In [8], the ℓ_1-SRACV method is based on a sparse representation of array covariance vectors, and applies the sparsity constraints to an ℓ_1-norm minimization problem to improving the DOA estimation performance. In [10], ℓ_1-SVD represents sparsely the signal subspace by left singular value decomposition. In [9], a low complexity sparse covariance-based DOA estimation method called LC-SRACV is proposed, which uses the Khatri-Rao (KR) product in a sparse signal representation framework to recover array covariance vectors of only one single measurement vector.

Comparing the subspace-based methods, except for not being sensitive to orthogonality of the signal and noise subspace, the sparse-representation-based DOA estimation approaches also have other superiorities. As known in [9], LC-SRACV extends the array aperture from M (the number of sensors) to $2M-1$ and increases the degrees of freedom. And it has much less computational cost than that of ℓ_1-SRACV and ℓ_1-SVD. The ℓ_1-SRACV DOA estimation method does not concern any knowledge of covariance array, and it can be applicable to an arbitrary array. ℓ_1-SVD [10] is not dependent on the knowledge of the noise covariance. However, there are obvious limitations in these sparse-based DOA estimation methods. For LC-SRACV, its most important limitation lies in the fact that the steering vectors must be the special structure of Vandermonde, and it is not suitable for UCA completely because the elements of overcomplete basis have not a clear monadic correspondance to direction samples. ℓ_1-SVD is dependence of the signal subspace singular vectors, in which the singular value decomposition (SVD) is necessary. Its computational complexity of ℓ_1-SVD has a close relationship with the number of incoming signals, which increases with the incoming signals. In addition, it is challenging to determine the regularization parameters when no knowledge of the noise or of sources is available. ℓ_1-SRACV adopts ℓ_1 penalty for sparsity and ℓ_2 penalty for each representation coefficient vector. Two-fold iterations make its computational cost higher than that of the formers.

These methods mentioned above are all manipulated in the element-domain. In the beamspace domain, the beamspace transform technique [19,20] is mainly adopted to solve the DOA estimation problem of UCA, which is the manifold separation technique [21] that can be used in an arbitrary array. This technique is a modal transform that maps the vectors of UCA to that of a virtual uniform linear array with Vandermonde structure. Thus, some DOA estimators with MUSIC in beamspace and derives, such as Real Beamspace MUSIC (RB-MUSIC) [16], are proposed, however, the estimator relies heavily on a priori known signal number, which has a close relationship with noise subspace decomposition, and has no capability of angular separation if the number of sources beyond the number of the sensors.

In this paper, we propose a low complexity sparse beamspace DOA estimation for UCA by vectorizing the array covariance vectors, called BS-ℓ_1-SRSMVS, which exploits a methodology combining the BT technique and sparse signal representation model of single measurement vectors in beamspace. In order to convert the UCA model to ULA-type model, a KR-based UCA signal model [22] is proposed by vectorization operation on the array covariance, the new array manifold can be decomposed into a product of a selection matrix and a Vandermonde structure with

the DOA information. Comparing the subspaced-method such as RB-MUSIC, the proposed method doesn't need know a priori knowledge of the number of sources and has higher angle resolution. Due to the centro-Hermitian characteristics of the steering vectors of virtual ULA, using Khatri-Rao product, the sparse vectors to be estimated can be recovered with single measurement vectors rather than multiple measurement vectors (MMVs) [23, 24] used in other sparse-based DOA estimation methods, such as ℓ_1-SVD and ℓ_1-SRACV. Therefore, it has lower computational complexity.

This paper is organized as follows. In Section 2, we overview the related works of DOA estimation based on sparse signal representation. In Section 3, we derive the steering vectors of the virtual ULA (VULA) in beamspace via the BT technique, and induce a dimension-reduction virtual array signal model for UCA based on Khatri-Rao product. Subsequently we propose a new sparse covariance-based beamspace DOA estimation method. In Section 4, we analyse the computional complexity of different methods theoretically. In section 5, we have some experiments, and the results verify the performance of the proposed method. Finally, Section 6 concludes the paper.

2 Related works

Here we focus on some DOA estimation methods based on sparse signal representation [8–10, 14]. The signal models are reconstructed using types of vectors, which are introduce in Section 2.1 and Section 2.2.

2.1 Singular Vectors of Data Matrix

In this case, the data matrix is generally processed in the element domain. Using the singular value decomposition transformation [10], a signal model composed of singular vectors is reconstructed, namely the singular vectors signal space. It is formulated as $\mathbf{Y}^{\mathrm{sv}} = \mathbf{A}\mathbf{S}^{\mathrm{sv}} + \mathbf{N}^{\mathrm{sv}}$, where $\mathbf{Y}^{\mathrm{sv}}$, $\mathbf{A}$, $\mathbf{S}^{\mathrm{sv}}$ and $\mathbf{N}^{\mathrm{sv}}$ is respectively data matrix of signals received, array manifold matrix, impinging signals and noise. $\mathbf{S}^{\mathrm{sv}}$ is a two-dimension matrix, which indexes rows by spatial dimension and columns by singular vector index. Thus the ℓ_2-norm of the i-th row vector $\widetilde{\mathbf{s}}_i$ of $\mathbf{S}^{\mathrm{sv}}$, i.e. $\widetilde{\mathbf{s}}_i^{(\ell_2)}$ (here $\widetilde{\mathbf{s}}_i$ is a scalar), corresponds to the sparsity of the spatial spectrum, where $i = 1, \ldots, Q$, Q is the number of signals. So the DOA estimation is converted to search the spatial spectrum of $\widetilde{\mathbf{s}}$ by minimizing

$$\|\mathbf{Y}^{\mathrm{sv}} - \mathbf{A}\mathbf{S}^{\mathrm{sv}}\|_{\mathrm{F}}^2 + \lambda \|\widetilde{\mathbf{s}}\|_1 \tag{1}$$

Where λ is weighted parameter, $\|\bullet\|_{\mathrm{F}}$ is Frobenius norm, $\widetilde{\mathbf{s}} = \left[\widetilde{\mathbf{s}}_1^{(\ell_2)}, \cdots, \widetilde{\mathbf{s}}_Q^{(\ell_2)}\right]$. It is obvious to see from (1) that the SVD transformation and ℓ_2-norm of the row-indexed singular vectors are necessary. Generally, using the optimization toolbox, (1) is transformed to

$$\min \|\widetilde{\mathbf{s}}\|_1 \ \text{ subject to } \ \|\mathbf{Y}^{\mathrm{sv}} - \mathbf{A}\mathbf{S}^{\mathrm{sv}}\|_{\mathrm{F}}^2 \leq \beta^2. \tag{2}$$

Where β is regularization parameter, the choice of which is still an open problem if no knowledge of sources is available.

2.2 Covariance Matrix Vectors of Signal Space

Another signal representation is the vectorized signal model based on the covariance matrix vectors. In [8], the signal model is represented as $\mathbf{R} = \widetilde{\mathbf{A}}(\theta)\mathbf{B}+\sigma^2\mathbf{I}_M$, where $\mathbf{R}$ is covariance matrix of array signals received, $\widetilde{\mathbf{A}}(\theta) = [\mathbf{a}(\theta_1), \cdots, \mathbf{a}(\theta_i), \cdots, \mathbf{a}(\theta_Q)]$ is overcomplete basis based on sensors array structure, where Q is the number of the overcomplete basis vectors, $\mathbf{I}_M$ is an $M \times M$ identity matrix, σ^2 is power of noise. $\mathbf{B} \in \mathbb{C}^{Q\times M}$ is the matrix composed of multiple measurement column vectors, which all share the same sparse structure. The nonzero elements of $\mathbf{B}$ is appeared in the same rows of the column vectors $\{\mathbf{b}^T\}_1^M$. Having solving ℓ_2-norm of $\mathbf{B}$ by rows, i.e. $\mathbf{b}_i^{(\ell_2)}(i = 1, \cdots, Q)$ (here $\mathbf{b}_i^{(\ell_2)}$ is a scalar), we can obtain a vector of $\mathbf{b} = \left[\mathbf{b}_1^{(\ell_2)}, \cdots, \mathbf{b}_Q^{(\ell_2)}\right]$, the nonzero element of which corresponds to certian vector $\mathbf{a}(\theta_i)$ of the overcomplete basis $\widetilde{\mathbf{A}}(\theta)$. The problem is expressed as

$$\min_{\mathbf{B}} \|\mathbf{b}\|_1 \text{ subject to } \mathbf{R} = \widetilde{\mathbf{A}}(\theta)\mathbf{B} + \sigma^2\mathbf{I}_M. \tag{3}$$

Having introduced the Lagrange multiplier η, (3) is transformed to

$$\min_{\mathbf{B}} \left\|\mathbf{W} \cdot \mathrm{vec}\left[\mathbf{R} - \widetilde{\mathbf{A}}(\theta)\mathbf{B} - \sigma^2\mathbf{I}_{\mathrm{M}}\right]\right\|_2^2 + \eta \|\mathbf{b}\|_1 . \tag{4}$$

where $\mathbf{W}$ is the weight matrix related to the covariance matrix $\mathbf{R}$, vec($\bullet$) denotes the vectorization operator.

Specially for a ULA, a derived mehod is presented in [9]. Having vectorizing the covariance matrix of $\mathbf{B}$, due to the centro-Hermitian property of column vectors of $\widetilde{\mathbf{A}}(\theta)$, (4) is transformed to

$$\min_{\mathbf{B}} \left\|\mathbf{W} \cdot \left[\mathrm{vec}(\mathbf{R}) - (\widetilde{\mathbf{A}}^*(\theta) \odot \widetilde{\mathbf{A}}(\theta))\mathbf{u} - \sigma^2\mathrm{vec}(\mathbf{I}_{\mathrm{M}})\right]\right\|_2^2 + \eta \|\mathbf{u}\|_1 \tag{5}$$

where $\odot$ represents the KR product and $(\bullet)^*$ denotes complex conjugate. Here $\mathbf{u}$ is the Q-sparse vector. Different from [8], the object to be optimizated is not a matrix but a vector.

3 Proposed method

In this section, we introduce our proposed method. In Section 3.1, we firstly derive the virtual array signal mode in beamspace by using beamspace transforming. And in Section 3.2, we introduce the covariance matrix representation by KR-product. In Section 3.3, we introduce the Sparse Covariance-based Beamspace DOA Estimation via single measurement vector.

3.1 Virtual Array Signal Model in Beamspace

Consider an array composed of M sensors located on a uniform circular array of radius r. There are $P(P < M)$ narrowband uncorrelated signals impinging on the array in the far-field. $\boldsymbol{\phi} = \{\phi_1, \phi_2, \cdots, \phi_P\}$ is the set of the incident angles of the signals. The observation data of UCA is formulated as

$$\mathbf{x}(t) = \mathbf{A}(\boldsymbol{\phi})\mathbf{s}(t) + \mathbf{n}(t), \quad t = 1, \cdots, N, \tag{6}$$

where $\mathbf{x}(t) = [x_1(t), x_2(t), \cdots, x_M(t)]^T$ is an $M \times 1$ noise-corrupted array snapshot vector, $(\bullet)^T$ is transpose operator. $\mathbf{s}(t) = [s_1(t), s_2(t), \cdots, s_P(t)]^T$ is a $P \times 1$ signal vector, and $\mathbf{n}(t) \in \mathbb{C}^M$ is assumed zero-mean Gaussian white noise. $\mathbf{A}(\boldsymbol{\phi}) = [\mathbf{a}(\phi_1), \mathbf{a}(\phi_2), \cdots, \mathbf{a}(\phi_P)] \in \mathbb{C}^{M \times P}$ is the array manifold matrix of the UCA, here $\mathbf{a}(\phi_p), p = 1, \cdots, P$ is an $M \times 1$ steering vector. It can be expressed as

$$\mathbf{a}(\phi_p) = \begin{bmatrix} e^{j\zeta\cos(\phi_p - \gamma_1)} \\ e^{j\zeta\cos(\phi_p - \gamma_2)} \\ \cdots \\ e^{j\zeta\cos(\phi_p - \gamma_M)} \end{bmatrix}, \tag{7}$$

where $j = \sqrt{-1}$, $\zeta = kr$ and wavenumber $k = 2\pi/\lambda$, here λ is the wavelength corresponding to the incident signals. $\gamma_{\mathrm{m}} = 2\pi(m-1)/M, (m = 1, 2, \cdots, M)$ are sensors' locations along the circumference of the UCA.

Assume that the signals $\{s_p(t)\}_{p=1}^P$ are uncorrelated for different sources, and also independent of $\mathbf{n}(t)$. The covariance matrix of the observation data $\mathbf{x}(t)$ is given by

$$\mathbf{R} = \mathrm{E}[\mathbf{x}(t)\mathbf{x}^H(t)] = \mathbf{A}(\boldsymbol{\phi})\mathbf{R}_{\mathrm{s}}\mathbf{A}^H(\boldsymbol{\phi}) + \sigma_n^2\mathbf{I}_M. \tag{8}$$

where $\mathbf{R}_{\mathrm{s}} = \mathrm{E}[\mathbf{s}(t)\mathbf{s}^H(t)]$ is the signal covariance matrix, whose diagonal elements are $\{\sigma_{sp}^2\}_{p=1}^P$. And σ_n^2 is the noise power. $\mathrm{E}(\bullet)$ and $(\bullet)^H$ are the expectation and the conjugate transpose operator respectively. $\mathbf{I}_M$ is an $M \times M$ identity matrix. In [9] and [25] , the dimension of the array manifold matrix is reduced from $M^2 \times P$ to $(2M-1) \times P$ by KR product. It works for ULA, but not for UCA. However, the recieved signal mode of a UCA can be transformed into that of a ULA-type array by synthesizing the beamspace manifold similar to that of a ULA using phase mode excitation of continuous circular aperture [19]. Thus a signal model of virtual ULA or ULA-type array can be obtained by using BT technique, which essentially takes discrete spatial sampling of far-field pattern resulting from all harmonics of array excitation (each harmonic means one phase mode, theoritically it ranges from $-\infty$ to $+\infty$. Actually the magnitude of harmonic decays super-exponentially with increasing harmonic order h, i.e. h-th phase mode. If h is large enough and reach a certain number H_e, the magnitude is asymptotically approaching zero) by incoming signals over continuous aperture of UCA [26]. The beamspace manifold synthesized by a beamformer $\mathbf{F}_e^H = \mathbf{C}_v\mathbf{V}^H$ [19] is given by

$$\mathbf{a}_e(\phi_p) = \mathbf{F}_e^H\mathbf{a}(\phi_p) = \mathbf{C}_v\mathbf{V}^H\mathbf{a}(\phi_p) \approx \sqrt{M}\mathbf{J}_\zeta\mathbf{d}(\phi_p), \tag{9}$$

where

$$\mathbf{C}_v = \mathrm{diag}\left\{j^{-H_e}, \ldots, j^{-1}, j^0, j^{-1}, \ldots, j^{-H_e}\right\}, \tag{10}$$

$$\mathbf{V} = \sqrt{M}\left[\mathbf{w}_{-H_e} : \cdots : \mathbf{w}_0 : \cdots : \mathbf{w}_{H_e}\right], \tag{11}$$

$$\mathbf{J}_\zeta = \mathrm{diag}\left[J_{H_e}(\zeta), \ldots, J_1(\zeta), J_0(\zeta), J_1(\zeta), \ldots, J_{H_e}(\zeta)\right], \tag{12}$$

where the matrices $\mathbf{C}_v$ and $\mathbf{J}_\zeta$ are $(2H_e+1)\times(2H_e+1)$ diagonal matrices. The matrix $\mathbf{V}$ is a normalized beamforming weight matrix that excites the array with a finite number of excitation modes. The modes that can be excited are $h \in [-H_e, H_e]$. Here a rule of thumb for determining H_e is given as $H_e \approx \zeta$ and H_e should satisfy $H_e < M/2$. The terms of $\{\mathbf{w}_h\}_{h=-H_e}^{H_e}$ are regarded as the spatial discrete sampling vectors corresponding to the far-field pattern, which is caused by the h-th phase mode along the continuous circular aperture. It is defined by

$$\mathbf{w}_h^H = \frac{1}{M}\left[e^{jh\gamma_1}, e^{jh\gamma_2}, \ldots, e^{jh\gamma_M}\right]. \tag{13}$$

$\mathbf{J}_\zeta$ is a matrix of Bessel functions, which's the diagonal elements' amplitudes taper symmetrically. From (9), we know that the steering vectors $\mathbf{a}_e(\phi_p)$ in beamspace is represented by the vector $\mathbf{d}(\phi_p)$, which contains the DOA information and can be expressed as

$$\mathbf{d}(\phi_p) = \left[e^{-jH_e\phi_p}, \ldots, e^{-j\phi}, 1, e^{j\phi}, \ldots, e^{jH_e\phi_p}\right]^T, \tag{14}$$

here $\sqrt{M}\mathbf{J}_\zeta\mathbf{d}(\phi_p)(p = 1, 2, ..., P)$ are ideal steering vectors of virtual ULA with Vandermonde structure.

The methodology of phase mode excitation-based beamformer offers the operation on transforming observation data in element space into that of beamspace. For the observation data illustrated in (6), using the methodology, we have $\mathbf{y}(t) \in \mathbb{C}^{M_e\times P}$, here $M_e = 2H_e + 1$ is the total number of excited modes. It is given by

$$\mathbf{y}(t) = \mathbf{F}_e^H\mathbf{x}(t) = \sqrt{M}\mathbf{J}_\zeta\mathbf{D}(\boldsymbol{\phi})\mathbf{s}(t) + \mathbf{F}_e^H\mathbf{n}(t). \tag{15}$$

From (15), we know that the observation data matrix $\mathbf{x}(t)$ of $M \times P$ dimensions in element-space is mapped into a dimension-reduction matrix $\mathbf{y}(t)$ of $M_e \times P$ dimensions in beamspace. And the term $\sqrt{M}\mathbf{J}_\zeta\mathbf{D}(\boldsymbol{\phi})\mathbf{s}(t)$ is a noise-free beamspace data matrix, which is given as a product of virtual array manifold $\mathbf{D}(\boldsymbol{\phi})$, the source vector $\mathbf{s}(t)$ and Bessel functions. Here $\mathbf{D}(\boldsymbol{\phi}) = [\mathbf{d}(\phi_1), \mathbf{d}(\phi_2), ..., \mathbf{d}(\phi_P)]$ has centro-Hermitian columns with Vandermonde structure. It is noticed that $\mathbf{F}_e^H$ is a unitary matrix that satisfies $\mathbf{F}_e^H\mathbf{F}_e = \mathbf{I}_{M_e}$. So the by-product $\mathbf{F}_e^H\mathbf{n}(t)$ of the transformation still remains a white Gaussian process. Thus, we have the covariance matrix of the observation data $\mathbf{y}(t)$. It is given by

$$\mathbf{R}_\mathbf{y} = M\mathbf{J}_\zeta\mathbf{D}(\phi)\mathbf{R}_\mathbf{s}\mathbf{D}^H(\phi)\mathbf{J}_\zeta + \sigma_n^2\mathbf{I}_{M_e}. \tag{16}$$

3.2 KR-Based Covariance Matrix Representation

In this subsection, we apply the KR subspace approach to DOA estimation [22] with virtual ULA and derive a new array model of KR virtual ULA. For the signal representation formulated in the above section, applying the vectorization operator on (16), we have a new array model expressed as

$$\mathbf{Y} := \mathrm{vec}(\mathbf{R}_\mathbf{y}) = M[(\mathbf{J}_\zeta^*\mathbf{D}^*(\boldsymbol{\phi})) \odot (\mathbf{J}_\zeta\mathbf{D}(\boldsymbol{\phi}))]\sigma_\mathbf{s}^2 + \sigma_n^2\mathbf{1}, \tag{17}$$

Here $\mathbf{1} = [\mathbf{e}_1^T, \mathbf{e}_2^T, ...\mathbf{e}_{M_e}^T]^T$, $\{\mathbf{e}_p\}_{l=1}^{M_e}$ is $M_e \times 1$ vector with one at the pth position and nought otherwise. The virtual array response matrix $(\mathbf{J}_\zeta^* \mathbf{D}^*(\boldsymbol{\phi})) \odot (\mathbf{J}_\zeta \mathbf{D}(\boldsymbol{\phi})) \in \mathbb{C}^{M_e^2 \times P}$can be formulated as

$$(\mathbf{J}_\zeta^* \mathbf{D}^*(\boldsymbol{\phi})) \odot (\mathbf{J}_\zeta \mathbf{D}(\boldsymbol{\phi})) = \mathbf{G}\mathbf{B}(\boldsymbol{\phi}), \tag{18}$$

here $\mathbf{B}(\boldsymbol{\phi}) \in \mathbb{C}^{(2M_e-1)\times P}$ is a dimension-reduced virtual array response matrix that expressed as

$$\mathbf{B}(\boldsymbol{\phi}) = [\mathbf{b}(\phi_1), \mathbf{b}(\phi_2), ..., \mathbf{b}(\phi_p), ...\mathbf{b}(\phi_P)] \tag{19}$$

where

$$\mathbf{b}(\phi_p) = [e^{-j(M_e-1)\phi_p}, ..., e^{-j\phi_p}, 1, e^{j\phi_p}, ...e^{j(M_e-1)\phi_p}]^T \tag{20}$$

and $\mathbf{G} \in \mathbb{C}^{M_e^2 \times (2M_e-1)}$ is given by

$$\mathbf{G} = (\mathbf{J}_\zeta \otimes \mathbf{J}_\zeta)\mathbf{H} \tag{21}$$

where $\otimes$ symbolises Kronecker product. Here $\mathbf{H}$ is the selection matrix given by

$$\mathbf{H} = [\mathrm{vec}(\mathbf{H}_{M_e-1}), \cdots, \mathrm{vec}(\mathbf{H}_1), \mathrm{vec}(\mathbf{H}_0), \mathrm{vec}(\mathbf{H}_1^T), \cdots, \mathrm{vec}(\mathbf{H}_{M_e-1}^T)] \tag{22}$$

with

$$\mathbf{H}_i = \begin{bmatrix} \mathbf{0}_{M_e-i} & \mathbf{I}_{M_e-i} \\ \mathbf{0}_{i,i} & \mathbf{0}_{i,M_e-i} \end{bmatrix}, i = 0, 1, ...M_e - 1. \tag{23}$$

Now (17) can be reformulated as below.

$$\mathbf{Y} = M\mathbf{G}\mathbf{B}(\boldsymbol{\phi})\sigma_{\mathrm{s}}^2 + \sigma_n^2\mathbf{1}. \tag{24}$$

From (24), we know that $\mathbf{Y}$ and $\sigma_{\mathbf{s}}^2$ are new observation vector and equivalent signal vector. The observation data $\mathbf{Y}$, vectorization of $\mathbf{R}_{\mathrm{y}}$, behaves like a new signal model. The virtual array response matrix $\mathbf{G}\mathbf{B}(\boldsymbol{\phi})$ is a new observation array, which has a larger aperture than that of the array which is not vectorized. $\sigma_{\mathbf{s}}^2$ is the signal vector, which describes the powers of each signal. σ_n^2 represents the power of noise. When no knowledge of the noise is available, σ_n^2 is estimated and given by the minimum of the eigenvalue of $\mathbf{R}_{\mathbf{y}}$. Thus (24) is expressed as a linear combination of the powers by any complete basis in the M_e^2 dimension vector space.

3.3 Sparse Covariance-based Beamspace DOA Estimation via Single Measurement Vector

Given the overcomplete basis $\{\mathbf{b}(\widetilde{\phi}_q)\}_{q=1}^{Q}(Q \gg M_e^2)$, where $\{\widetilde{\phi}_q\}_{q=1}^{Q}$ are the discrete samples of potential incident directions of signals in spatial domain. Here denote the vector of $\{\widetilde{\phi}_q\}_{q=1}^{Q}$by $\widetilde{\boldsymbol{\phi}}$. Therefore (24) can be reformulated as a SMV form

$$\mathbf{Y} = M\mathbf{G}\mathbf{B}(\widetilde{\boldsymbol{\phi}})\mathbf{u} + \sigma_n^2\mathbf{1}, \tag{25}$$

which is essentially a underdetermined signal reconstruction problem. We can estimate the DOAs of the signals by recovering the sparse vector $\mathbf{u}$ of a single measurement vector $\mathbf{Y}$. At this point, if the grid resolution of $\widetilde{\boldsymbol{\phi}}$ is dense enough, then some P column vectors of $\mathbf{B}(\widetilde{\boldsymbol{\phi}})$ is approaching to or equal to $\{\mathbf{b}(\phi_p)\}_{p=1}^{P}$. Correspondly, an estimated P-sparse vector $\hat{\mathbf{u}}$, whose nonzero elements are close to or equal to $\{\sigma_{sp}^2\}_{p=1}^{P}$ is estimated. In theory, (25) can be solved by the following constraint ℓ_1 optimization that expressed as [27]

$$\min_{\hat{\mathbf{u}}} ||\hat{\mathbf{u}}||_1 \ s.t. \ \hat{\mathbf{Y}} = M\mathbf{GB}(\widetilde{\boldsymbol{\phi}})\hat{\mathbf{u}} + \sigma_n^2\mathbf{1}, \tag{26}$$

here $\hat{\mathbf{u}}$ and $\hat{\mathbf{Y}}$ are the estimates of $\mathbf{u}$ and $\mathbf{Y}$ respectively. From (26), we know that if $\hat{\mathbf{u}} \to \sigma_{\mathbf{s}}^2$, then $\hat{\mathbf{Y}} \to \mathbf{Y}$. And some $\{\widetilde{\phi}\}_{p=1}^{P}$ are very close to the DOAs of the incident signals. We know that the estimate error of $\hat{\mathbf{Y}} - \mathbf{Y}$ with the weighted matrix of $\mathbf{W} = \frac{1}{N}\mathbf{R}_{\mathbf{y}}^T \otimes \mathbf{R}_{\mathbf{y}}$ follows asymptotically normal (AsN) distribution [27], which is given by

$$\mathbf{W}^{-\frac{1}{2}}[\hat{\mathbf{Y}} - M\mathbf{GB}(\widetilde{\boldsymbol{\phi}})\mathbf{u} - \sigma_n^2\mathbf{1}] \sim \mathrm{AsN}(\mathbf{0}, \mathbf{I}_{M_e^2}) \tag{27}$$

Using least-squares criterion, the weighted estimate error follows asymptotic chi-square distribution with M_e^2 degree-of-freedoms. It is formulated as

$$\| \mathbf{W}^{-\frac{1}{2}}[\hat{\mathbf{Y}} - M\mathbf{GB}(\widetilde{\boldsymbol{\phi}})\mathbf{u} - \sigma_n^2\mathbf{1}] \|_2^2 \sim As\chi^2(M_e^2), \tag{28}$$

here $\hat{\mathbf{Y}} = \mathrm{vec}(\hat{\mathbf{R}}_{\mathbf{y}})$, where $\hat{\mathbf{R}}_{\mathbf{y}} = \frac{1}{N}\sum_{t=1}^{N}\mathbf{y}(t)\mathbf{y}^H(t)$. It is taken as the estimate of $\mathbf{Y}$. Thus a modified DOA estimation mode is derived from (26) by introducing the parameter of β, which makes the inequality $\| \mathbf{W}^{-\frac{1}{2}}(\hat{\mathbf{Y}} - \mathbf{Y}) \|_2^2 < \beta^2$ hold with a high probability $\tilde{\mathrm{p}}$. It specifies how much estimate error we wish to allow. It is expressed as follows

$$\Pr(\chi^2(\mathrm{M_e^2}) \leqslant \beta^2) = \tilde{\mathrm{p}}, \quad \beta = \sqrt{\chi_{\tilde{\mathrm{p}}}^2(\mathrm{M_e^2})} \tag{29}$$

where $\Pr(\bullet)$ denotes the probability distribution. Then (26) can be expressed as

$$\min_{\hat{\mathbf{u}}} \|\hat{\mathbf{u}}\|_1 \ s.t. \ \| \mathbf{W}^{-\frac{1}{2}}(\hat{\mathbf{Y}} - M\mathbf{GB}(\widetilde{\boldsymbol{\phi}})\hat{\mathbf{u}} - \sigma_n^2\mathbf{1}) \|_2^2 \leq \beta^2 \tag{30}$$

Using the Matlab convex optimization toolbox, the P-sparse vector $\hat{\mathbf{u}}$ can be obtained. we can plot the peaks versus the directions and determine the DOA of the signal expected. The proposed algorithm is summarized in Algorithm 1.

Remark From (17), we know that $\mathrm{krank}(\mathbf{GB}(\boldsymbol{\phi})) \geq \min\{P, 2 \times \mathrm{krank}(\mathbf{J}_\zeta\mathbf{D}(\boldsymbol{\phi})) - 1\}$. Here $\mathrm{krank}(\mathbf{J}_\zeta\mathbf{D}(\boldsymbol{\phi})) = M_e$, where $\mathrm{krank}(\bullet)$ denotes the *Kruskal rank* (see definition in [15] for details). It means that every collection of $2M_e - 1$ column vectors of $\mathbf{GB}(\boldsymbol{\phi})$ is linearly independent and there exits a set of $2M_e$ column vectors linearly dependent. That is $\mathrm{Spark}(\mathbf{GB}(\boldsymbol{\phi})) = 2M_e$. The constraint condition of ℓ_1 optimization for a unique P-sparse vector $\mathbf{u}$ is $\mathrm{Spark}(\mathbf{GB}(\boldsymbol{\phi})) > 2P$. i.e. $2H_e + 1 > P$, which means that the DOA estimator for virtual ULA with H_e modes can handle $2H_e$ signals at most.

Algorithm 1: BS-ℓ_1-SRSMVS

input : the received signal $\mathbf{x}(t)$; the radius r of UCA; the wavelength λ_i of signal $s_i(t)$,$i = 1, 2, ...P$; the sensor number M

output: the P-sparse vector $\hat{\mathbf{u}}$

determing the beamspace manifold $\mathbf{F}_e^H$;
for $i \leftarrow 1$ **to** P **do**
  $H_e \leftarrow$ `CalculatePhaseModeNumber`(λ_i, r);
  $\zeta \leftarrow 2\pi r/\lambda_i$;
  if $H_e > M/2$ **then**
    `break`;
  end
end
calculating $\mathbf{C}_v$,$\mathbf{V}$ and $\mathbf{J}_\zeta$;
$\mathbf{F}_e^H \leftarrow$ `MatrixMultiplcation`($\mathbf{C}_v$, $\mathbf{V}$);
reconstructing the KR-based signal model;
$\mathbf{y}(t) \leftarrow$ `MatrixMultiplcation`($\mathbf{F}_e^H$, $\mathbf{x}(t)$);
$\hat{\mathbf{R}}_\mathbf{y} \leftarrow \frac{1}{N}\sum_{k=1}^{N}\mathbf{y}(t)\mathbf{y}^H(t)$;
$\hat{\mathbf{Y}} \leftarrow$ `Vec`($\hat{\mathbf{R}}_\mathbf{y} - \sigma_n^2\mathbf{I}_M$); `// reconstruct KR-based noise-free signal model`
construct overcomplete basis;
calculating the selection matrix $\mathbf{H}$;
$\mathbf{G} \leftarrow$ `MatrixMultiplcation(Kron(`$\mathbf{J}_\zeta$,$\mathbf{J}_\zeta$`)`, $\mathbf{H}$);
for $i \leftarrow 1$ **to** Q **do**
  $\mathbf{b}(\widetilde{\phi}_i)$;
end
$\mathbf{B}(\widetilde{\boldsymbol{\phi}}) \leftarrow [\mathbf{b}(\widetilde{\phi}_i)]_1^Q$;
obtaining the overcomplete basis $\mathbf{GB}(\widetilde{\boldsymbol{\phi}})$;
convex optimation;
$\mathbf{W} \leftarrow \frac{1}{\sqrt{N}}$`Kron`($\hat{\mathbf{R}}_\mathbf{y}^{-\frac{T}{2}}$, $\hat{\mathbf{R}}_\mathbf{y}^{-\frac{1}{2}}$); `// calculate weighted matrix`
initialize $\boldsymbol{\Xi}$, β;
$\beta \leftarrow$ `Chisquare`($2H_e + 1$, $\tilde{\mathrm{p}}$);
while `Norm`($\boldsymbol{\Xi}$) $< \beta$ **do**
  $\boldsymbol{\Xi} \leftarrow$ `MatrixMultiplcation`($\mathbf{W}$, $\hat{\mathbf{Y}} - \mathbf{GB}(\widetilde{\boldsymbol{\phi}})\hat{\mathbf{u}}$);
  if `min`($\|\hat{\mathbf{u}}\|_1$) **then**
    `break`;
  end
end
`return` $\hat{\mathbf{u}}$

4 Computational complexity analysis

The methods of ℓ_1-SVD and ℓ_1-SRACV have advantages of being applicable for an arbitrary array, however, they have much higher complexity than the proposed method that is specialized for UCA. Besides optimational calculation of objective function, for ℓ_1-SVD, the computational load is mainly stressed on singular value decomposition of observation data and the computational cost of ℓ_1-SRACV is concerned on eigenvalue decomposition (EVD) of covariance matrix. The proposed method lower the computational complexity through reducing the dimension of observation data using BT technique. Table 1 shows the computational complexity of different processes using ℓ_1-SVD, ℓ_1-SRACV, BS-ℓ_1-SRSMVS and RB-MUSIC. We know that a priori number of incoming signals should be necessary for ℓ_1-SVD and RB-MUSIC. So their computional costs have a close relationship with P. ℓ_1-SRACV is not susceptible to the number P of signals but the number M of sensors. Here $M > P$ and $M > 2H_e$. From Table 1, we know that the computational complexity of the proposed method is $O((2H_e+1)MN+(2H_e+1)^2N+(2H_e+1)^3+(4H_e+2)(4H_e+1)(2H_e+1)Q+Q^3)$, which covers the process of beamspace transformation, covariance matrix, eigenvalue decomposition (skipping or skimming if the noise power is known in advance), the construction of objective function via weighted matrix $\mathbf{W}^{-\frac{1}{2}}$ and optimational calculation without spectral search. Considering estimation accuracy of DOA, we know that $Q \gg M$, thus it is the most-weighted factor that results in major time consuption in the estimators. Simplifying the complexity of ℓ_1-SVD , ℓ_1-SRACV and the proposed method, they are respectively $O(P^3Q^3)+O((MP+1))Q$, $O(M^3Q^3)+O((M^3+M^2)Q)$, $O(Q^3)+32(H_e^3Q)$. Provided that the grid resolution of directional samples Q is constant, we know that the higher of M or P is, the larger the computational complexity will be. In addition, due to the dimension-reduction process of UCA, the computational complexity of covariance matrix and EVD of the proposed method is lower than that of ℓ_1-SVD and ℓ_1-SRACV. Thus its compuational load is much less than ℓ_1-SVD and ℓ_1-SRACV. Comparing the subspace-based methods as RB-MUSIC, our proposed method has inferiority of higher computational complexity, but the superiority of angle separation that conventional methods are incomparable, which has been illustrated in Section 5.

Table 1: Complexity Comparison of Different Methods

Procedures	Complexity			
	ℓ_1-SVD	ℓ_1-SRACV	RB-MUSIC	BS-ℓ_1-SRSMVS
Beamspace transform	×	×	$O((2H_e+1)MN)$	$O((2H_e+1)MN)$
Covariance matrix	×	$O(M^2N)$	$O((2H_e+1)^2N)$	$O((2H_e+1)^2N)$
EVD/SVD	$O(M^3)$	$O(M^3)$	$O((2H_e+1)^3)$	$O((2H_e+1)^3)$
Objective function	$O(MQP+MP+QP+Q)$	$O(M^3+M^3Q+M^2Q)$	×	$O((4H_e+1)^2(2H_e+1)+(4H_e+1)(2H_e+1)Q)$
Convex optimization	$O((PQ)^3)$	$O((MQ)^3)$	×	$O(Q^3)$
Spectral search	×	×	$O(2(2H_e+1)^2Q-2(2H_e+1)PQ+(2H_e+1)Q)$	×

5 Results and discussion

In this section, we evaluate the performance of the proposed method by simulations with different settings. We run these dependent experiment trials on a PC with a 2.4GHz processor of Intel Core i5-6200U, 8G of RAM. The software environment is Matlab 2017b running on Windows 10 operating system.

5.1 Phase Mode Choice and Mapping Error

In this subsection, we run some experiments to have an analysis of the relationship between amplitudes of steering vector and phase modes. In addition, the mapping error of steering vector on transforming UCA to virtual ULA is defined, and its relationship with phase mode is given as well. Here taking a 9-sensor UCA and a 16-sensor UCA as examples, the amplitudes of steering vector of different phase modes are depicted in Fig.1. For the 9-sensor UCA, we can see from the Fig.1(a) and Fig.1(b) that the maximal amplitudes of grating lobes of $H_e = 4$ are 4dB lower than that of $H_e = 10$ and 3dB lower than that of $H_e = 15$, respectively. For the 16-sensor UCA, Fig.1(c) and Fig.1(d), it is also noticed that the maximal amplitudes of grating lobes of $H_e = 15$ and $H_e = 31$ are about 5dB and 7dB higher than that of $H_e = 7$ ($H_e > 8$), where λ is $0.8r$ if $He = 7$, λ is $0.4r$ if $He = 15$. Meanwhile, we can see that with the phase mode increasing, the main lobe of $H_e = 15$, $H_e = 31$ is almost 10° and 14° narrower than that of $H_e = 7$ for the 16-sensor UCA, and the main lobe of $H_e = 10$, $H_e = 15$ is about 18° and 22° narrower than that of $H_e = 4$ for the 9-sensor UCA. Taking the phase mode of $H_e = 7$ for the 16-sensor UCA with radius r=1 for example, the circumferential spacing between adjacent array sensors is 0.39, which is larger than half the wavelength when $H_e = 15$. It means that the phase ambiguity of steering vectors could be existed on the process of the transforming UCA to virtual ULA if the maximum of phase mode does not satisfy $He < M/2$.

Using (9), we can get a steering vector with Vandermonde structure of a new ULA-type array. Under the constraints of number of sensors and interelement spacing, the steering vectors of this new array are the finite approximation of the far-field pattern of UCA with finite phase mode excitation. It is noted that this constraint of $M > 2H_e$ is similar to the Nyquist sampling criterion in which H_e defines the maximum spatial frequency component in the array excitation [26]. When $H_e = \zeta$, it is obvious that the circumferential spacing between adjacent sensors of the UCA is less than 0.5λ, which sufficiently avoids spatial aliasing in virtual ULA. The approximation leads to mapping error. Here we define it as

$$\epsilon_h(H_e) = \frac{\|\mathbf{a}(\phi_p) - \sqrt{M}\mathbf{F}_e\mathbf{J}_\zeta\mathbf{d}(\phi_p)\|_F}{\|\mathbf{a}(\phi_p)\|_F}. \tag{31}$$

Suppose $H_e = \lfloor n\zeta \rfloor, n \in \mathbb{Q}^+$, which $\mathbb{Q}^+$ is the positive rational number set. Fig.2 shows that mapping error $\epsilon_h(H_e)$ decreases as H_e (or n) increases and r/λ decreases. The plots show the mapping error as a function of phase mode H_e of the UCA with M being respectively 48, 40, 32, 24, 16 and λ being correspondingly $4.19r$, $5.02r$, $6.27r$, $8.35r$, $12.49r$. Their circumferential spacings between adjacent sensors of the UCAs are all less than 0.5λ. From Fig.2, we know that $\epsilon_h(H_e) \approx 0$ (i.e., the minimum

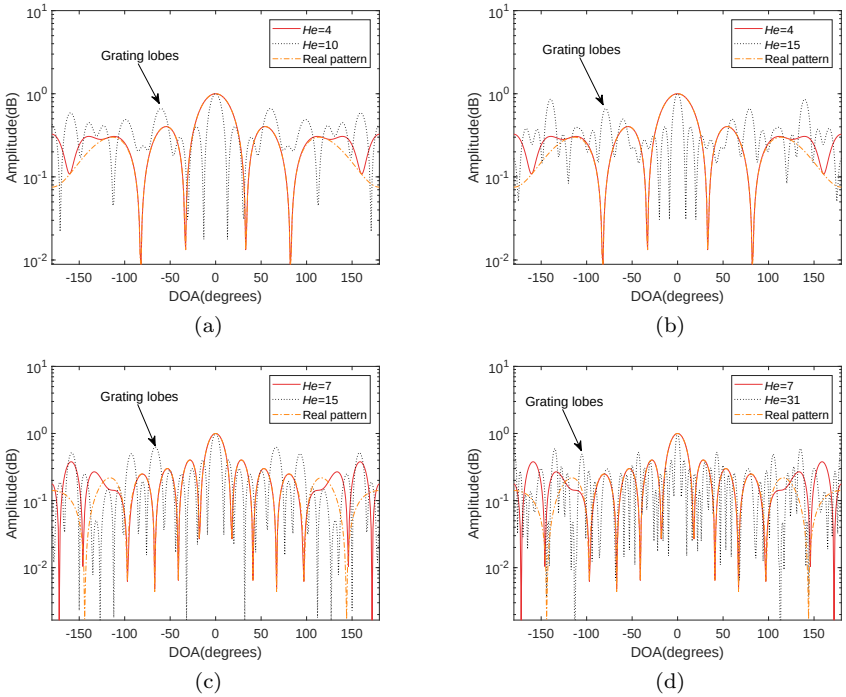

Figure 1: Comparison of pattern amplitudes for M-sensor UCA. (a) M=9, He is 4, 10, correspondlingly $r = 0.6\lambda$, 1.5λ . (b) M=9, He is 4, 15, correspondlingly $r = 0.4\lambda$, 1.5λ. (c) M=16, He is 7, 15, correspondlingly $r = 0.8\lambda$, 0.4λ. (d) M=16, He is 7, 31, correspondlingly $r = 0.8\lambda$, 0.2λ.

is approaching to 10^{-15}) if H_e approximates to ∞. Accordingly the interelement spacing is approaching to 0 theoretically, and at this point (9) represents the far-field pattern of the continuous circular aperture. So if extending H_e sufficiently to large, the mapping error is almost negligible.

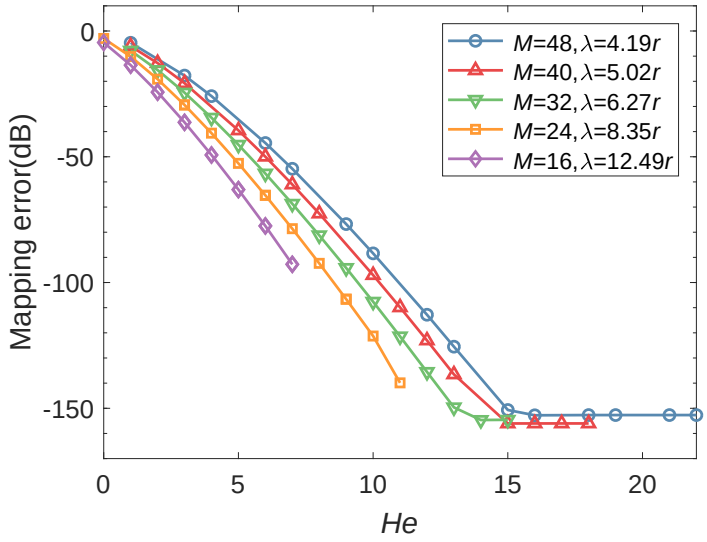

Figure 2: Mapping error as a function of phase mode H_e for UCA with various r/λ, in which the circumferential spacing between adjacent sensors of UCA is $0.0313r$. The maximum of phase mode is respectively 7, 11, 15, 18, 22, correspondingly M=16, 24, 32, 40, 48.

5.2 Spectra of the Proposed Method

We consider the cases of two uniform circular arrays of M=7 and M=11 sensors and testify the performance of BS-ℓ_1-SRSMVS comparing with Capon beamformer and RB-MUSIC.

Fig.3 shows the spatial spectra of BS-ℓ_1-SRSMVS, Capon beamformer and RB-MUSIC. One case is investigated, where the true DOAs of actual narrowband signals impinging on the array are respectively 30°, 90°, 150°, 210°, 270°, 330°. And the simulation results are plotted in Fig.3(a), in which number of sensors is $M = 7$, $r/\lambda = 0.5$, SNR = 0dB and the number of snapshots is $N = 1000$, the parameter of β is 7.07. The other case which $M = 11$, $r/\lambda = 0.5$, SNR = 20dB and $N = 2000$ is examinated. The sources impinge on the array from the directions of 10°, 40°, 70°, 100°, 130°, 160°, 190°, 220°, 250°, 280°. The simulation results are depicted in Fig.3(b), in which the parameter of β is 7.28. As is known that the maximum phase mode of the 7-sensor UCA is 3 and that of 11-sensor UCA is 5. From the plots, we know that RB-MUSIC and BS-ℓ_1-SRSMVS are both capable of estimating all these signals, however, BS-ℓ_1-SRSMVS has higher resolution and output SNR than those of RB-MUSIC and Capon beamformer. We also notice that the maxima of DOAs estimated of these two cases are 6 and 10. It is indicated that BS-ℓ_1-SRSMVS can estimate $2H_e$ signals regardless of the number of sensors on the premise of

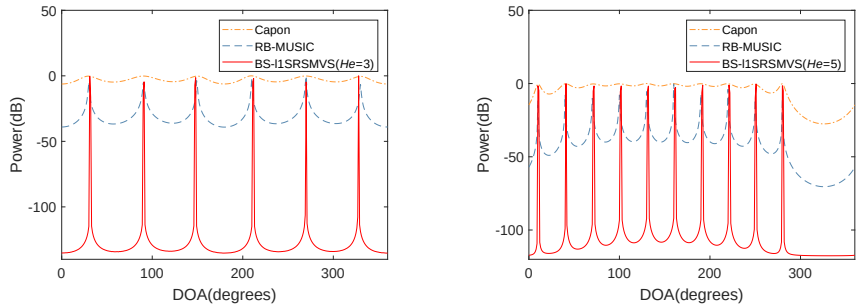

Figure 3: Spatial spectra for Capon beamformer , RB-MUSIC and BS-ℓ_1-SRSMVS. (a) M=7, r/λ=0.5, N=1000, SNR=0, H_e=3, DOAs=(30°, 90°, 150°, 210°, 270°, 330°). (b) M=11, r/λ=0.5, N=2000, SNR=20, H_e=5, DOAs=(10°, 40°, 70°, 100°, 130°, 160°, 190°, 220°, 250°, 280°.).

$M > 2H_e$. Thus for a M-sensor UCA, the proposed method can estimated at most $M-1$ signals.

5.3 Performance Evaluation

In this subsection, we carry out independent trials to verify the performance of our proposed method provided that the phase mode of H_e is 5, 9, 11 respectively. The number of sensors is 12, 24, 36. The radius r of the UCA is 0.5λ. The root mean squared error is defined as RMSE $= \sqrt{\mathrm{E}\left\{\frac{1}{Q}\sum_{j=1}^{Q}(\hat{\theta}_j-\theta_j)^2\right\}}$, where $\hat{\theta}_j$ indicates the estimated DOA and θ_j denotes the ture DOA. Q is the number of independent Monte Carlo experiments with $Q = 500$. The SNR ranges from -10dB to 22dB. On the transforming of UCA in element space to virtual ULA in beamspace, the mapping error decreases as H_e increases. The RMSEs results are shown in Fig.4. As is seen that the RMSEs decreases as the phase mode increases, and with the SNR increasing, it decreases as well.

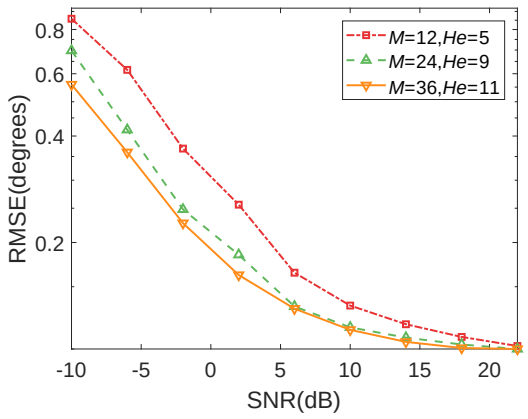

Figure 4: RMSE performance versus SNR with different phase mode.

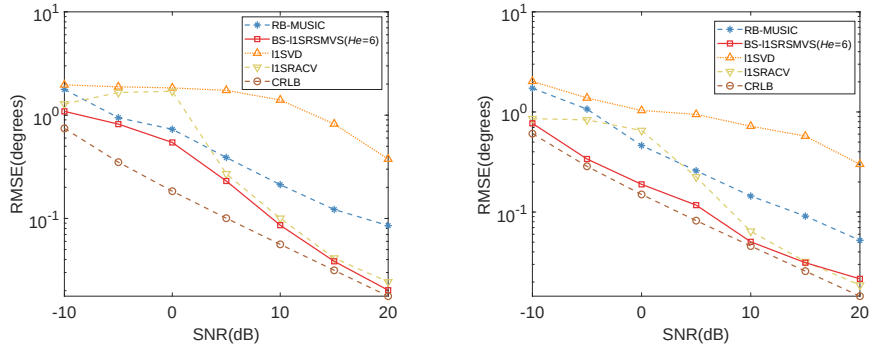

Figure 5: RMSE comparison for varying SNR with RB-MUSIC, BS-ℓ_1-SRSMVS, ℓ_1-SVD, ℓ_1-SRACV and CRLB. (a) M=13, N=500. (b) M=13, N=1000.

We evaluate the RMSE of the proposed method and compare that with other mothods and the stochchastic Cramér-Rao lower bound(CRLB) [28], in which the number of sensors is 13 and the radius of the UCA is 0.5λ. Fig.5 shows the RMSE of different methods under different SNR conditions. The statistical results are obtained by runing the Monte-Carlo simulation of 500 independent trials, where the number of snapshots are respectively 500, 1000 and the the SNR is varied from -10dB to 20dB in 5dB steps. The plots are shown in Fig.5(a) and Fig. 5(b). With the SNRs increasing, it can be seen that the mean-square error of the proposed method is statistically less than that of ℓ_1-SVD, ℓ_1-SRACV and RB-MUSIC.

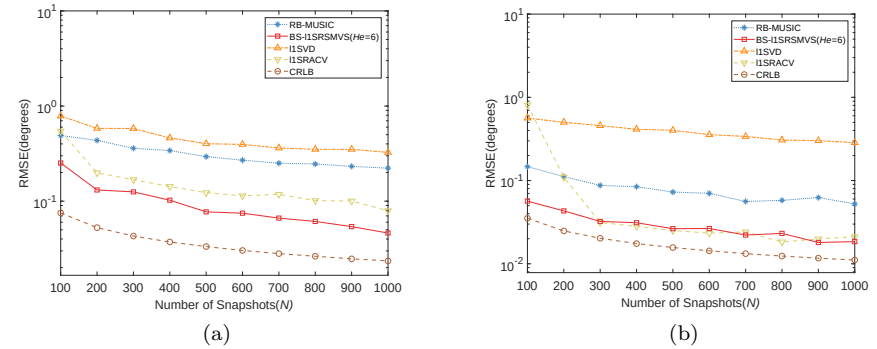

Figure 6: RMSE comparison versus snapshots with RB-MUSIC, BS-ℓ_1-SRSMVS, ℓ_1-SVD, ℓ_1-SRACV and CRLB. (a) M=13, SNR=0dB. (b) M=13, SNR=10dB.

The RMSE varying with the number of snapshots is plotted in Fig.6, from which the proposed method and ℓ_1-SRACV both provide lower RMSEs than other methods. However, the proposed method yields much smaller RMSEs than ℓ_1-SRACV when the number of snapshots is less than 300. It outperforms ℓ_1-SVD and ℓ_1-SRACV for the sparse-based DOA estimation methods as a whole.

5.4 Performance of Angular Separation

We compare the spectra of the proposed method to that of MUSIC and RB-MUSIC, which are applied in element sapce and beamspace, ℓ_1-SVD and ℓ_1-SRACV. The simulation is based on an 13-element uniform circular array with half-wavelength circumferential element spacing. The total number of snapshots N is 200 and 2000 respectively. The grid resolution of overcomplete basis is 0.1° with 1800 points sampled from 0° to 180°.

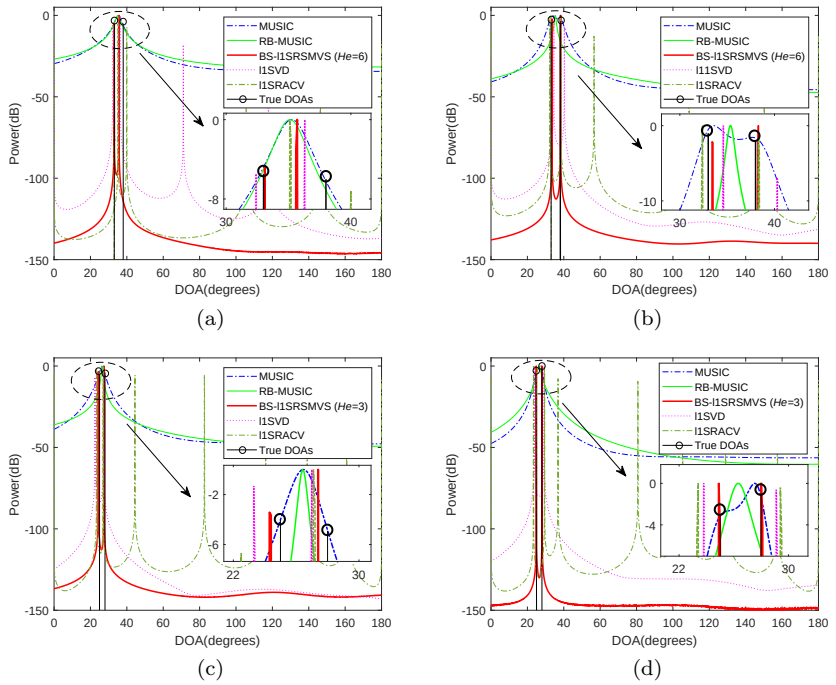

Figure 7: Angular separation versus SNR of different methods, M=13, r/λ=0.5. (a) SNR=0dB, N=2000, DOAs=$(33°, 38°)$. (b) SNR=10dB, N=2000, DOAs=$(33°, 38°)$. (c) SNR=20dB, N=200, DOAs=$(25°, 28°)$. (d) SNR=30dB, N=200, DOAs=$(25°, 28°)$.

Fig.7 shows the angular resolution versus SNR using different methods. The two sources are spaced closely, they spaced 5° in Fig.7(a) and Fig.7(b), and they are close to 3° in Fig.7(c) and Fig.7(d). From the results, we know that the subspace-based MUSIC merges the two peaks, whereas our proposed method, ℓ_1-SVD and ℓ_1-SRACV are capable of resolving the two sources. From Fig.7(a) and Fig.7(b), we know that even if the decrease of the SNR, ℓ_1-SVD and ℓ_1-SRACV still has an excellent performance of angle separarion, but if SNR decreases to 0 dB, ℓ_1-SVD produces spurious peaks [6]. And ℓ_1-SRACV produces spurious peaks as well if improper regularization parameters. However, the proposed method still has the perfect separation capability and ideal DOA estimation accuracy even if the number of the signals is unknown.

5.5 Comparison of Computational Complexity

In this subsection, we compare the CPU time of ℓ_1-SVD, ℓ_1-SRACV and that of our proposed method by plotting the CPU time versus the number of snapshots, array sensors and sources. The results are shown in Fig.8.

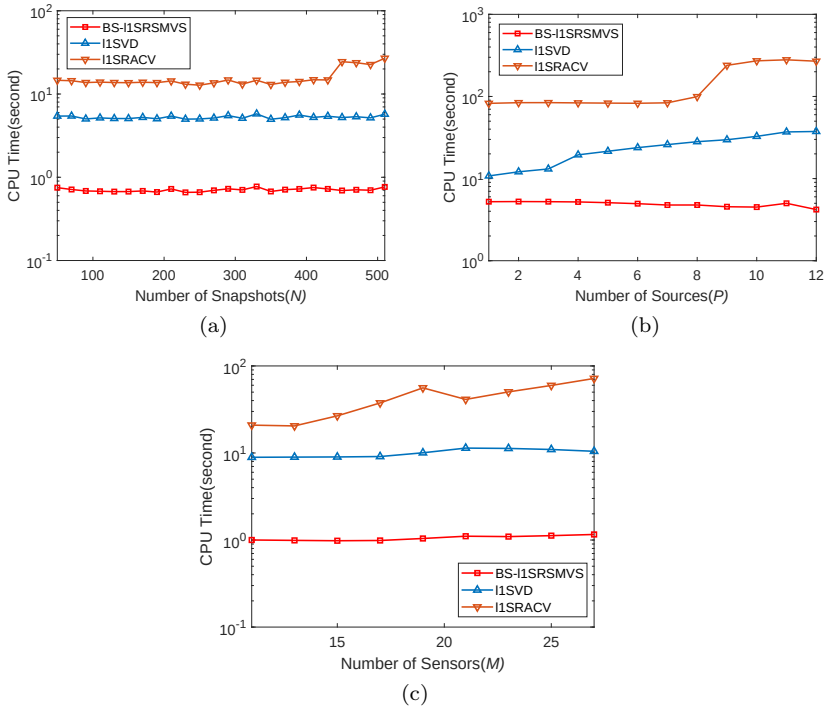

Figure 8: CPU time comparisons of BS-ℓ_1-SRSMVS, ℓ_1-SVD,ℓ_1-SRACV. (a) CPU time versus snapshots N, $M = 18$, r/λ=0.5, SNR = 20dB. (b) CPU time versus number of sources P, $M = 28$, r/λ=0.5, SNR = 20dB. (c) CPU time versus number of sensors M, H_e=5, $N = 500$, r/λ=0.5, SNR = 20dB.

Fig.8(a) shows CPU time cost versus snapshots using different methods. Here assume SNR = 20dB, $M = 18$, DOA = 66°, Q = 180, number N of snapshots ranges from 50 to 510. The DOA estimate is measured from 100 Monte Carlo runs. As is seen from the plot, the proposed method has much less time cost than ℓ_1-SVD and ℓ_1-SRACV. In Fig.8(b), we plot the CPU time cost of different methods with the number of sources P increasing. The SNR is 20dB, the number M of sensors is 28, the snapshots are assumed 100 and Q is 360. The DOAs of sources ranges from 10° to 340° with 30° angle spacing between two adjacent sources. As we know from Section IV, the computational complexity of the proposed method has nothing to do with source numbers but the overcomplete basis. Thus we can see that even if the number of the source increases, the CPU time of the proposed method has never increased dramatically all the time. The CPU time cost of ℓ_1-SVD is mainly dependent of the number of sources. If the number of sources increases from 1 to 12, accordingly the CPU time rangs from 10.77 seconds to 37.46 seconds. Fig.8(c) shows CPU time versus the number of sensors using different methods. The SNR is 20dB, $M = 11, 13, \cdots, 27$, the snapshots are 500. The DOA of one

incoming signal is assumed 55°. Comparing the CPU time costs of ℓ_1-SVD and ℓ_1-SRACV, the proposed method has obvious advantages of lower computational complexity. In the case that phase mode H_e is fixed at the same value, the steering vectors are dimension-reduced to He. Thus we know that the CPU time of our proposed method is not relevant to the number of M but with phase mode H_e, while that of ℓ_1-SRACV does increase with M. From the simulation, we know that the computational cost of the proposed method is nearly a tenth that of ℓ_1-SVD and ℓ_1-SRACV.

6 Conclusion

In this paper, a low complexity sparse covariance-based beamspace DOA estimation method for UCA is presented. In the proposed method, the virtual ULA-like array signal model is obtained by using beamspace transform, which get a array model with Vandermonde structure. And then, applying the vectorization operation on the covariance matrix of the new signal model, a dimension-reduction signal model is formulated, which greatly reduces the computational complexity. The proposed method is verified by simulations, the results show that it is not only has better DOA resolution performance than subspace-based methods in low SNR, but also has low computational complexity comparing other sparse-like DOA estimation methods.

Acknowledgements
The authors thank the anonymous reviewers for their enlightening comments and careful reviews, which helped improve the manuscript.

Funding
This work was supported in part by The National Key Research and Development Program of China under Grant 2016YFB0502001.

Abbreviations
DOA: Direction-of-arrival; UCA: Uniform circular array; SMV: Single measurement vector; BT: Beamspace transform; ULA: Uniform linear array; SNR: Signal-to-noise ratio; MUSIC: Multiple signal classification; RB-MUSIC: Real Beamspace MUSIC; KR: Khatri-Rao; MMV: Multiple measurement vector; VULA: Virtual ULA; SVD: Singular value decomposition; EVD: Eigenvalue decomposition.

Competing interests
The authors declare that they have no competing interests.

Authors' contributions
All authors contributed to the conception and design of the experiments and the interpretation of simulation results. ZD wrote the software, performed the experiments and data analysis, and wrote the first draft of the manuscript. TW substantially revised the manuscript. DZ and LG give some helpful experimental instructions and guidances. All authors read and approved the final manuscript.

Author details
[1]Wireless Network Positioning and Communication Integration Research Center, School of Electronic Engineering, Beijing University of Posts and Telecommunications, Beijing, 100876 China. [2]The 54th Research Institute of CETC, 050081 Shijiazhuang, China. [3]State Key Laboratory of Public Big Data, Guizhou Big Data Academy , Guizhou University, 550025 Guiyang, China.

References

1. Godara, L.C.: Application of antenna arrays to mobile communications. ii. beam-forming and direction-of-arrival considerations. Proceedings of the IEEE **85**(8), 1195–1245 (1997)
2. Zheng, Z., Wang, W., Meng, H., So, H.C., Zhang, H.: Efficient beamspace-based algorithm for two-dimensional doa estimation of incoherently distributed sources in massive mimo systems. IEEE Transactions on Vehicular Technology **67**(12), 11776–11789 (2018)
3. Amin, M.G., Bhalla, N.: Minimum bias spatial filters for beamspace direction-of-arrival estimation. Journal of the Franklin Institute **335**(1), 35–52 (1998)
4. Esfandiari, M., Vorobyov, S.A., Alibani, S., Karimi, M.: Non-iterative subspace-based doa estimation in the presence of nonuniform noise. IEEE Signal Processing Letters **26**(6), 848–852 (2019)
5. Yang, L., Yang, Y., Zhang, Y.: Subspace-based direction of arrival estimation in colored ambient noise environments. Digital Signal Processing **99**, 102650 (2020)

6. Xia, Y., Kanna, S., Mandic, D.P.: Maximum likelihood parameter estimation of unbalanced three-phase power signals. IEEE Transactions on Instrumentation and Measurement **67**(3), 569–581 (2018)
7. Mecklenbrauker, C.F., Gerstoft, P.: Maximum-likelihood doa estimation at low snr in laplace-like noise. In: 2019 27th European Signal Processing Conference (EUSIPCO), pp. 1–5 (2019)
8. Yin, J., Chen, T.: Direction-of-arrival estimation using a sparse representation of array covariance vectors. IEEE Transactions on Signal Processing **59**(9), 4489–4493 (2011)
9. He, Z.Q., Liu, Q.H., Jin, L.N., Ouyang, S.: Low complexity method for doa estimation using array covariance matrix sparse representation. Electronics Letters **49**(3), 228–230 (2013)
10. Malioutov, D., Cetin, M., Willsky, A.S.: A sparse signal reconstruction perspective for source localization with sensor arrays. IEEE Transactions on Signal Processing **53**(8), 3010–3022 (2005)
11. Yang, X., Ko, C.C., Zheng, Z.: Direction-of-arrival estimation of incoherently distributed sources using bayesian compressive sensing. IET Radar, Sonar Navigation **10**(6), 1057–1064 (2016)
12. Fuchs, J.: On the application of the global matched filter to doa estimation with uniform circular arrays **5**, 3089–30925 (2000)
13. Liu, Z., Huang, Z., Zhou, Y., Liu, J.: Direction-of-arrival estimation of noncircular signals via sparse representation. IEEE Transactions on Aerospace and Electronic Systems **48**(3), 2690–2698 (2012)
14. Cai, J., Wu, B., Li, P., Liu, W.: A sparse representation based doa estimation algorithm for a mixture of circular and noncircular signals using sparse arrays, 1–5 (2017)
15. Liu, C., Liao, G.: Robust capon beamformer under norm constraint. Signal Processing **90**(5), 1573–1581 (2010)
16. Schmidt, R.: Multiple emitter location and signal parameter estimation. IEEE Transactions on Antennas and Propagation **34**(3), 276–280 (1986)
17. Yan, F.-G., Shuai, L., Wang, J., Shi, J., Jin, M.: Real-valued root-music for doa estimation with reduced-dimension evd/svd computation. Signal Processing **152**, 1–12 (2018)
18. Fu, H., Abeywickrama, S., Yuen, C., Zhang, M.: A robust phase-ambiguity-immune doa estimation scheme for antenna array. IEEE Transactions on Vehicular Technology **68**(7), 6686–6696 (2019)
19. Mathews, C.P., Zoltowski, M.D.: Eigenstructure techniques for 2-d angle estimation with uniform circular arrays. IEEE Transactions on Signal Processing **42**(9), 2395–2407 (1994)
20. Zheng, Z., Wang, W., Meng, H., So, H.C., Zhang, H.: Efficient beamspace-based algorithm for two-dimensional doa estimation of incoherently distributed sources in massive mimo systems. IEEE Transactions on Vehicular Technology **67**(12), 11776–11789 (2018)
21. Belloni, F., Richter, A., Koivunen, V.: Doa estimation via manifold separation for arbitrary array structures. IEEE Transactions on Signal Processing **55**(10), 4800–4810 (2007)
22. Cao, M.-Y., Huang, L., Qian, C., Xue, J.-Y., So, H.C.: Underdetermined doa estimation of quasi-stationary signals via khatrirao structure for uniform circular array. Signal Processing **106**, 41–48 (2015)
23. Cotter, S.F., Rao, B.D., Kjersti Engan, Kreutz-Delgado, K.: Sparse solutions to linear inverse problems with multiple measurement vectors. IEEE Transactions on Signal Processing **53**(7), 2477–2488 (2005)
24. Chen, J., Huo, X.: Theoretical results on sparse representations of multiple-measurement vectors. IEEE Transactions on Signal Processing **54**(12), 4634–4643 (2006)
25. Ma, W., Hsieh, T., Chi, C.: Doa estimation of quasi-stationary signals with less sensors than sources and unknown spatial noise covariance: A khatrirao subspace approach. IEEE Transactions on Signal Processing **58**(4), 2168–2180 (2010)
26. Belloni, F., Koivunen, V.: Beamspace transform for uca: Error analysis and bias reduction. IEEE Transactions on Signal Processing **54**(8), 3078–3089 (2006)
27. Candes, E.J., Tao, T.: Near-optimal signal recovery from random projections: Universal encoding strategies? IEEE Transactions on Information Theory **52**(12), 5406–5425 (2006)
28. Stoica, P., Nehorai, A.: Performance study of conditional and unconditional direction-of-arrival estimation. IEEE Transactions on Acoustics, Speech, and Signal Processing **38**(10), 1783–1795 (1990). doi:10.1109/29.60109

Figures

Figure 1: Comparison of pattern amplitudes when phase mode of He is 7, 15, correspondlingly $r/\lambda = 1.25$, 2.5, and that of real pattern for the 16-sensor UCA of the radius r=1.

Figure 2: Mapping error as a function of phase mode H_e for UCA with various r/λ, in which the circumferential spacing between adjacent sensors of UCA is $0.0313r$. The maximum of phase mode is respectively 7, 11, 15, 18, 22, correspondingly M=16, 24, 32, 40, 48.

Tables

Figure 3: Spatial spectra for MUSIC, RB-MUSIC and BS-ℓ_1-SRSMVS. (a) M=7, r/λ=0.5, N=1000, SNR=0, H_e=3, DOAs=(30°, 90°, 150°, 210°, 270°, 330°). (b) M=11, r/λ=0.5, N=2000, SNR=20, H_e=5, DOAs=(10°, 40°, 70°, 100°, 130°, 160°, 190°, 220°, 250°, 280°.).

Figure 4: RMSE versus SNR with different phase mode.

Figure 5: RMSE comparison for varying SNR with RB-MUSIC, BS-ℓ_1-SRSMVS, ℓ_1-SVD, ℓ_1-SRACV and CRLB. (a) M=13, N=500. (b) M=13, N=1000.

Figure 6: RMSE comparison versus snapshots with RB-MUSIC, BS-ℓ_1-SRSMVS, ℓ_1-SVD, ℓ_1-SRACV and CRLB. (a) M=13, SNR=0dB. (b) M=13, SNR=10dB.

Figure 7: Angular separation versus SNR of different methods, M=13, r/λ=0.5. (a) SNR=0dB, N=2000, DOAs=$(33°, 38°)$. (b) SNR=10dB, N=2000, DOAs=$(33°, 38°)$. (c) SNR=20dB, N=200, DOAs=$(25°, 28°)$. (d) SNR=30dB, N=200, DOAs=$(25°, 28°)$.

Table 1: Complexity Comparison of Different Methods

Procedures	Complexity			
	ℓ_1-SVD	ℓ_1-SRACV	RB-MUSIC	BS-ℓ_1-SRSMVS
Beamspace transform	×	×	$O((2H_e+1)MN)$	$O((2H_e+1)MN)$
Covariance matrix	×	$O(M^2N)$	$O((2H_e+1)^2N)$	$O((2H_e+1)^2N)$
EVD/SVD	$O(M^3)$	$O(M^3)$	$O((2H_e+1)^3)$	$O((2H_e+1)^3)$
Objective function	$O(MQP+MP+QP+Q)$	$O(M^3+M^3Q+M^2Q)$	×	$O((4H_e+1)^2(2H_e+1)+(4H_e+1)(2H_e+1)Q)$
Convex optimization	$O((PQ)^3)$	$O((MQ)^3)$	×	$O(Q^3)$
Spectral search	×	×	$O(2(2H_e+1)^2Q-2(2H_e+1)PQ+(2H_e+1)Q)$	×

Figures

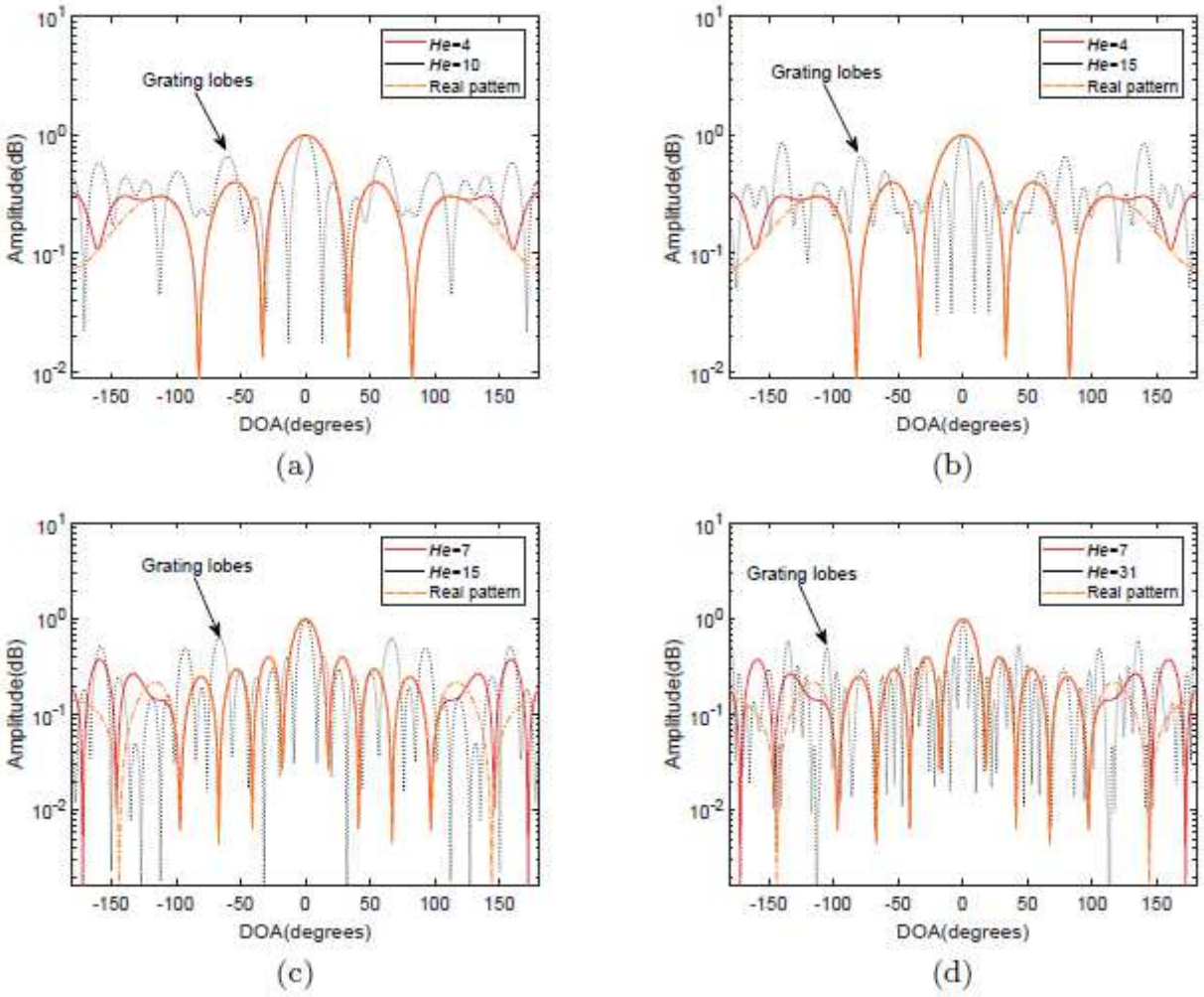

Figure 1

See the Manuscript Files section for the complete figure caption.

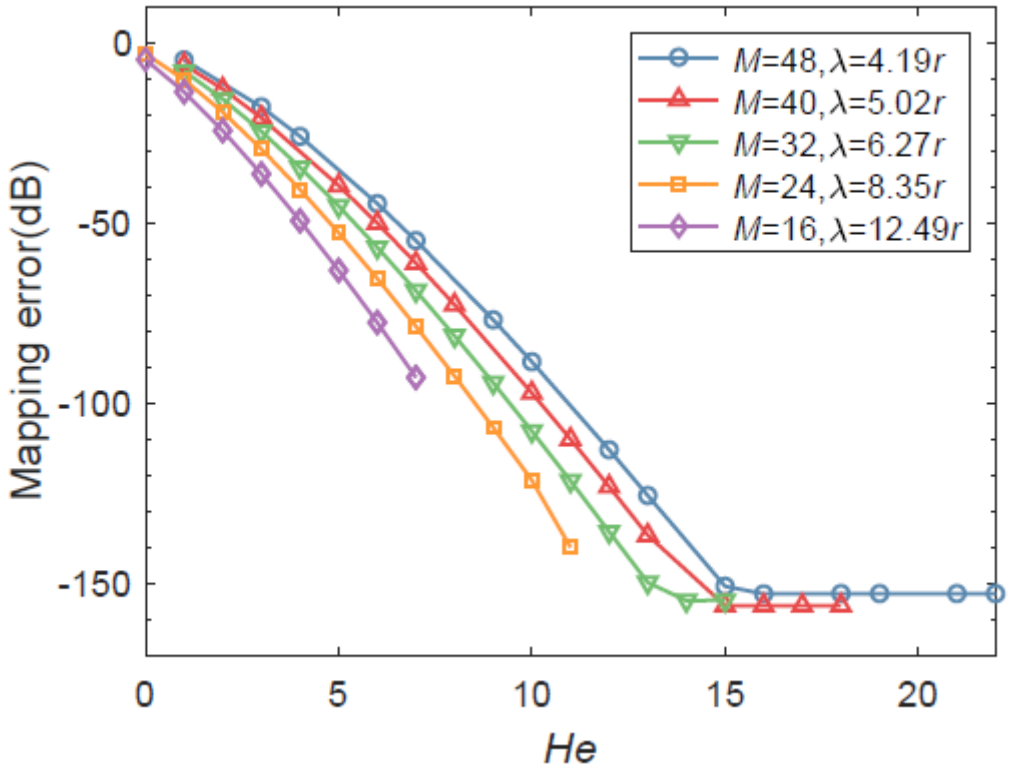

Figure 2

See the Manuscript Files section for the complete figure caption.

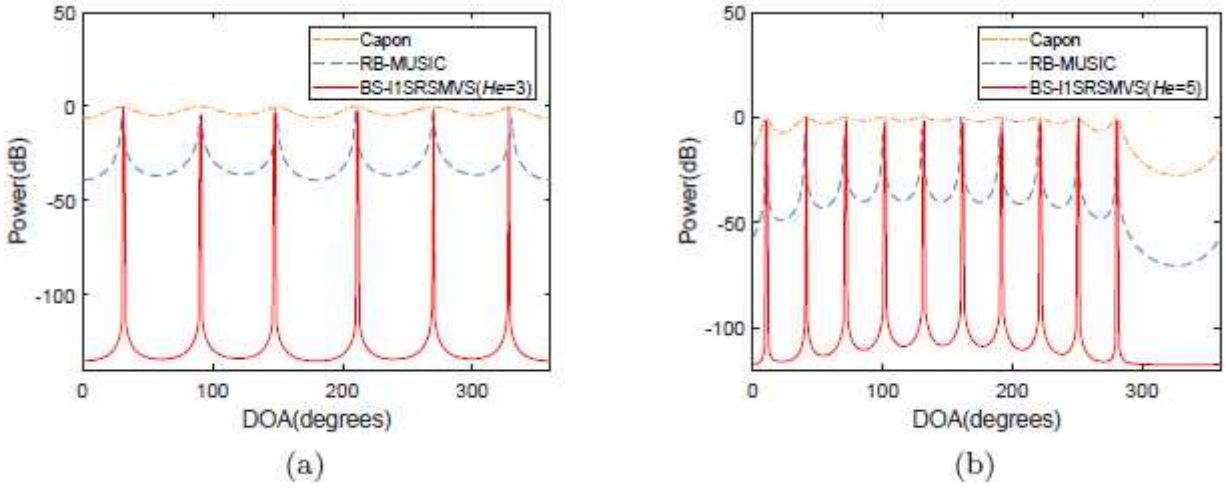

Figure 3

See the Manuscript Files section for the complete figure caption.

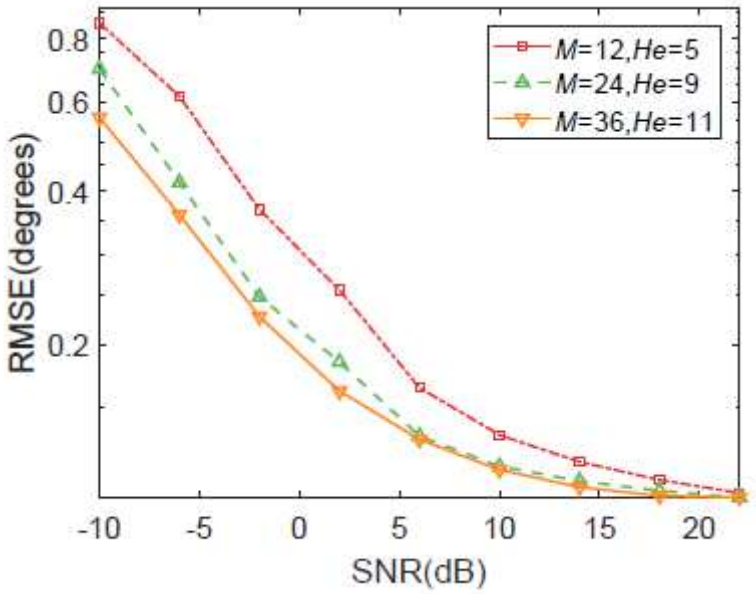

Figure 4

See the Manuscript Files section for the complete figure caption.

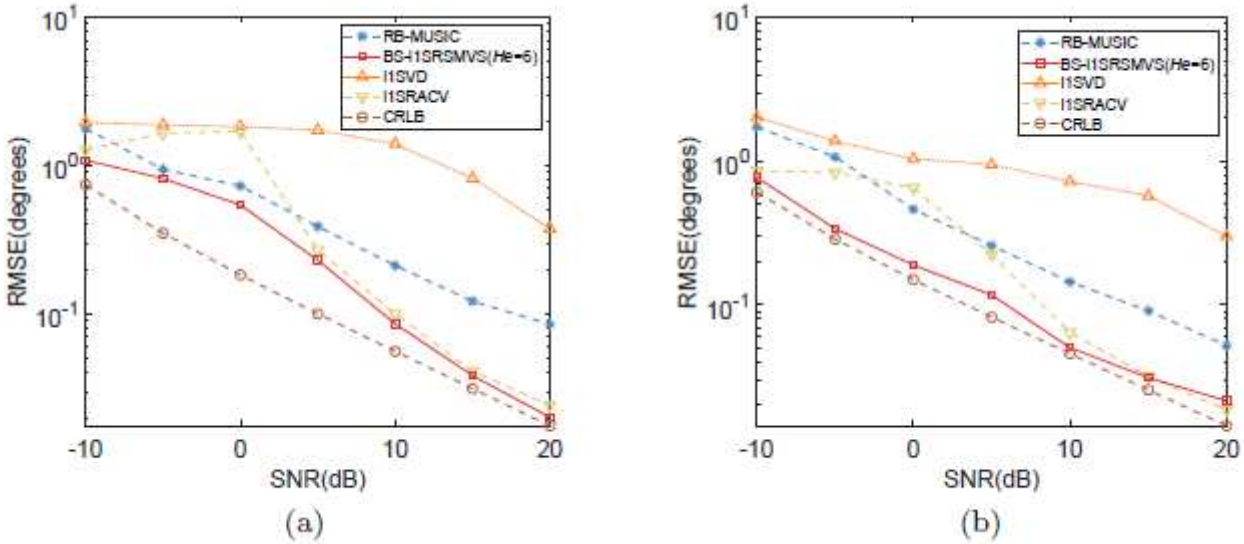

Figure 5

See the Manuscript Files section for the complete figure caption.

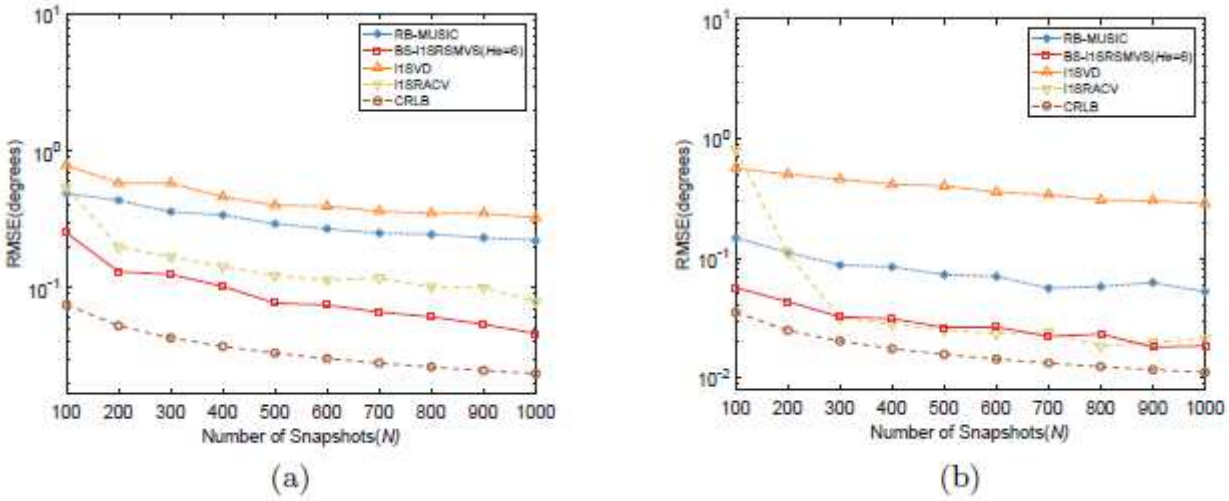

Figure 6

See the Manuscript Files section for the complete figure caption.

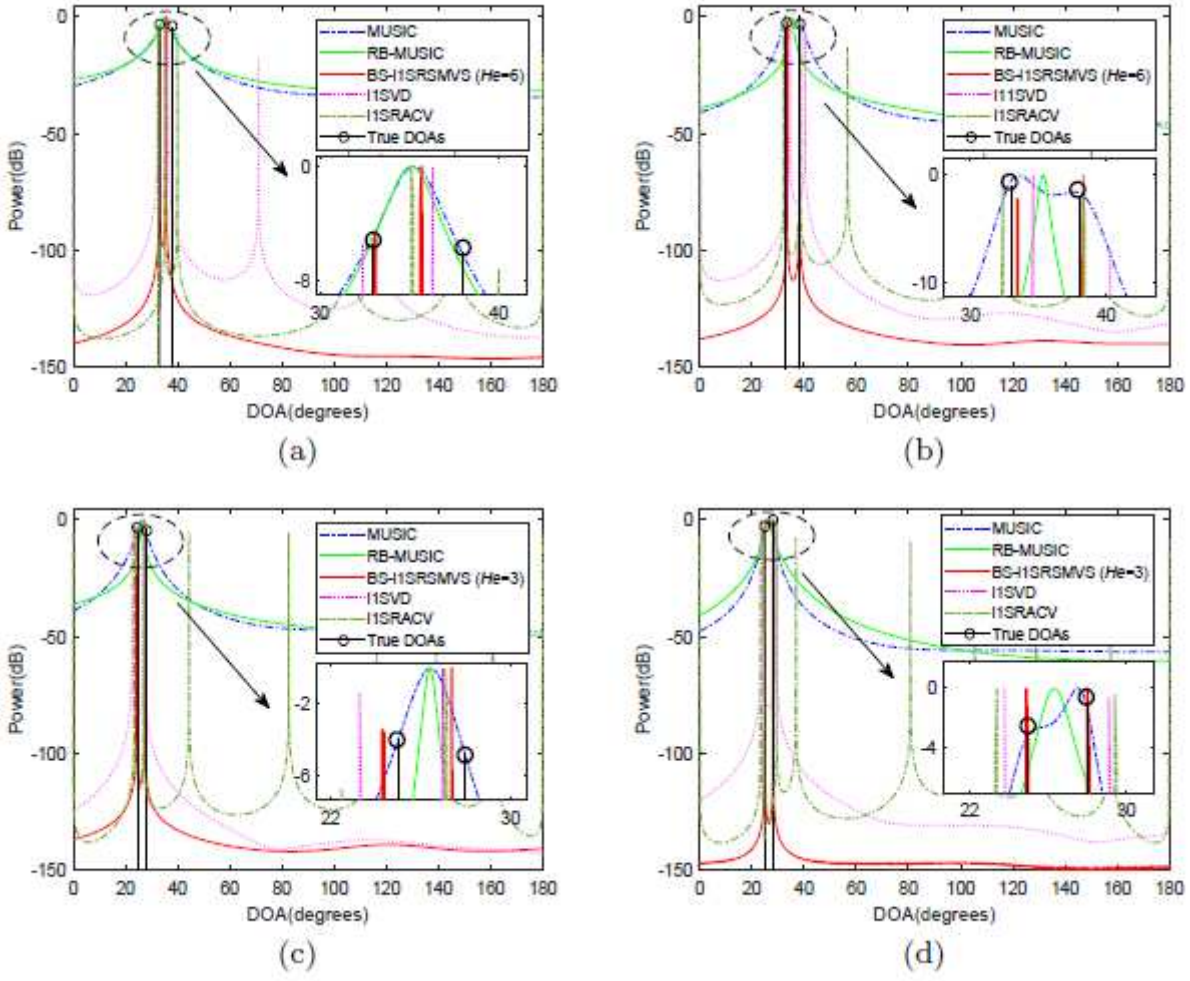

Figure 7

See the Manuscript Files section for the complete figure caption.

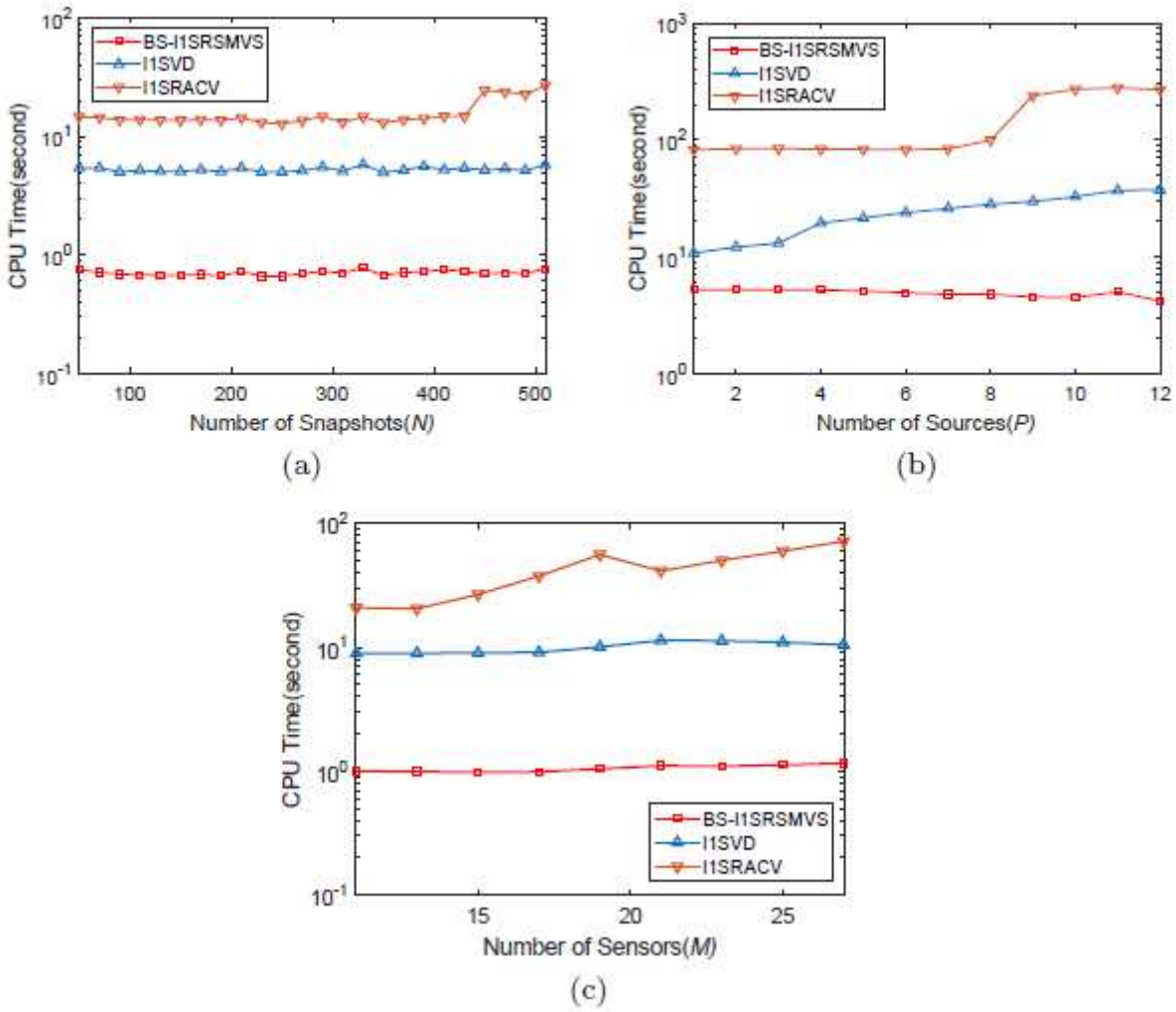

Figure 8

See the Manuscript Files section for the complete figure caption.